LA-UR- 08-6859

Approved for public release;
distribution is unlimited.

Title:	Precipitation of radiation belt electrons by EMIC waves, observed from ground and space
Author(s):	V. K. Jordanova, LANL, ISR-1 (see attached for additional authors)
Intended for:	Geophysical Research Letters

Form 836 (7/06)

Precipitation of radiation belt electrons by EMIC waves, observed from ground and space

Y. Miyoshi (1), K. Sakaguchi (1), K. Shiokawa (1), D. Evans (2), J. Albert (3), M. Connors (4), and V. Jordanova (5)

(1) Solar-Terrestrial Environment Laboratory, Nagoya University, Nagoya 464-8601, Japan
(2) NOAA/SWPC, Boulder, CO 80305, USA
(3) AFRL, Hanscom Air Force Base, MA 01731-3010, USA
(4) Centre for Science, Athabasca University, Alberta T9S 3A43, Canada
(5) Los Alamos National Laboratory, Los Alamos, NM 87545, USA.

Index term
2774: Radiation belts
2772: Plasma waves and instabilities
7867: Wave/particle interactions
2720: Energetic particles: trapped

Keywords
Outer radiation belt
EMIC
Wave-particle interactions

Abstract.

We show evidence that left-hand polarised electromagnetic ion cyclotron (EMIC) plasma waves can cause the loss of relativistic electrons into the atmosphere. Our unique set of ground and satellite observations shows coincident precipitation of ions with energies of tens of keV and of relativistic electrons into an isolated proton aurora. The coincident precipitation was produced by wave-particle interactions with EMIC waves near the plasmapause. The estimation of pitch angle diffusion coefficients supports that the observed EMIC waves caused coincident precipitation of both ions and relativistic electrons. This study clarifies that ions with energies of tens of keV affect the evolution of relativistic electrons in the radiation belts via cyclotron resonance with EMIC waves, an effect that was first theoretically predicted in the early 1970's.

1. Introduction

Populations of relativistic electrons in the radiation belts vary greatly with geomagnetic disturbance [e.g., Reeves et al., 2003; Miyoshi and Kataoka, 2005] and they are a major source of damage to space vehicles [e.g., Baker et al., 1987]. In order to know when and how much these populations of relativistic electrons increase, it is important to elucidate not only the cause of acceleration of relativistic electrons but also the cause of their loss from the radiation belts.

Several loss processes of relativistic electrons of the outer belt have been proposed [e.g; Millan and Thorne, 2007]. Relativistic electrons precipitate into the earth's atmosphere through pitch angle scattering caused by plasma waves, which is an important loss process in the outer belt. Whistler mode waves are essential for both non-adiabatic acceleration of relativistic electrons and pitch angle scattering [e.g., Lyons and Thorne, 1973; Li et al., 2007], and recent studies have shown that acceleration caused by whistler mode waves is very important for the flux enhancements of relativistic electrons in the outer belt [e.g., Horne, 2007; Miyoshi et al., 2003, 2007].

Left-hand polarized EMIC waves exist in the outer belt and usually precipitate ions with energies of tens of keV [Cornwall et al., 1970; Jordanova et al., 2001], generating the proton aurora in the upper atmosphere [Sakaguchi et al., 2007; Jordanova et al., 2007]. Resonance between EMIC waves and moderately energetic electrons is not possible because of their opposite polarisations. Theory suggests that EMIC waves can resonate with electrons when the energy of electrons becomes sufficiently high for the electrons to be relativistic [Thorne and Kennel, 1971; Lyons and Thorne, 1972; Horne and Thorne, 1998]. It is predicted that precipitation of relativistic electrons takes place near the dusk-side plasmapause, where EMIC waves are typically generated by ions with energies of tens of keV [Cornwall et al., 1970; Erlandson and Ukhorskiy, 2001; Meredith et al., 2003; Jordanova et al., 2008], and observations of MeV electron precipitation from ground and satellites have been suggestive of electron scattering caused by EMIC waves [Lorentzen et al., 2000; Millan et al., 2002; Sandanger et al., 2007]. However, it has not been possible thus far to confirm whether EMIC waves actually cause electron precipitation on the basis of particle observations alone. We describe here unique simultaneous ground and satellite observations of MeV electron precipitation caused by EMIC waves.

2. Observation

At about 0500 UT on September 5, 2005, we observed an isolated proton aurora in the southern sky at Athabasca, Canada, as shown in Figure 1a. Figure 1b shows an image of the proton aurora at the

wavelength of the Hβ (Hydrogen Balmer β) line obtained by averaging images captured from 0430 to 0500 UT with an all-sky cooled CCD imager at Athabasca [Shiokawa et al., 1999]. The stable isolated proton auroral arc, shown by the red rectangle, was observed just south of the zenith. The latitudinal width of the proton aurora was ~1 deg.

Simultaneously, we recorded magnetic pulsations with an induction magnetometer at Athabasca. The pulsations were observed continuously from 0230 to 0800 UT, during the recovery phase of a moderate geomagnetic storm. The sinusoidal nature of the pulsations is clear from Figure 2a, and results of a spectrum analysis shown in Figure 2b indicate that pulsations in the frequency range of 0.5-0.9 Hz are dominant. The three vertical lines in the figure indicate hydrogen, helium, and oxygen gyro-frequencies calculated from a geomagnetic field model [Tsyganenko, 2002a, b] for the geomagnetic equator along the magnetic field line of the observed proton aurora. The dominant frequency of the observed pulsations is between the helium and oxygen gyro-frequencies at the geomagnetic equator, indicating that the pulsations are helium-band EMIC waves that have propagated from the geomagnetic equator. Related observations [Sakaguchi et al., 2007, 2008] have shown the expected link between isolated proton auroras, pitch angle scattering of ions caused by EMIC waves, and resulting ion precipitation, which are consistent with previous studies[Sørras et al., 1980; Yahnina et al., 2000, 2003].

A unique opportunity to identify other precipitating particles and extend such observations to include high-energy electrons was realised when the low-altitude POES-17 (formally NOAA-17) satellite passed over Athabasca during this event. The dashed line of Figure 1b shows the POES-17 footprint trajectory during the overpass, mapped from satellite altitude of 800 km to the ionosphere along the magnetic field line, and transiting the eastern part of the proton arc. The POES satellite measures ions in six energy bands from 30 keV to more than 6900 keV, as well as electrons in three integrated energy ranges of >30 keV, >100 keV, and >300 keV. Separate particle detector telescopes observe locally mirroring particles returning to the magnetosphere via the magnetic mirror force, as well as particles precipitating into the atmosphere [Evans and Greer, 2000].

Figure 3 shows the precipitating (red) and trapped (black) ion and electron count rates observed by the POES-17 satellite over Athabasca together with the emission profile of Hβ (Figure 3a), with the POES footprint shown in the label. The black line in Figure 3b indicates the 30-80 keV ion count rates obtained from the telescope viewing the near locally mirroring particles along the satellite trajectory. Trapped ions of 30-80 keV were distributed over a wide magnetic latitude (MLAT) range from 50 deg to 70 deg, and high count rates of over 1000/s were seen in a MLAT range of 59 deg to 62 deg. The precipitation of 30-80 keV ions (red line in Figure **3b**) showed an isolated peak from

04:58:35 UT to 04:58:50 UT when the satellite footprint was just crossing the proton aurora, as shown in Figure 3a. The latitudinal width of the ion precipitation region was less than 1 deg, which is consistent with the proton aurora observations. As reported previously [Sakaguchi et al., 2007, 2008], isolated proton auroras observed at Athabasca usually show very good temporal correspondence with the appearance and disappearance of EMIC waves. Moreover, the gyro-frequencies estimated at the geomagnetic equator along the magnetic field line of the proton aurora agree well with the observed EMIC frequencies. It is therefore concluded that the observed EMIC waves scattered energetic ions into the atmosphere to cause the proton aurora. Similar ion precipitation was seen in the 80-240 keV energy range but not at energies higher than 240 keV. The fluxes of both trapped and precipitating protons above 240 keV were too small to be observable [see Figure 3 of Sakaguchi et al., 2007].

The POES-17 footprint was conjugate to the outer belt during the event, as shown by the locally mirroring electrons with energies between 300 keV and a couple of MeV (black line in Figure 3c). No significant precipitation of electrons below a couple of MeV (red line in Figure 3c) was found at 04:58-04:59 UT when EMIC waves were observed associated with the proton precipitation. Absence of precipitation was also observed for lower energy electrons of 30-100 keV and 100-300 keV, while significant fluxes of trapped electrons existed at those energy ranges [see Figure 3 of Sakaguchi et al., 2007].

Although the POES-17 satellite does not have sensors designed specifically to observe MeV electrons, the ion telescopes respond to relativistic electrons. A case of significant count rates in the nominal >6900 keV proton energy channel of the ion telescopes but no response in the 2400-6900 keV proton energy channel would represent an unphysical proton energy spectrum, and a detector response of that character is interpreted as being due to >800 keV electrons. In addition, an ion sensor designed to monitor >16 MeV protons over a wide acceptance angle will respond to electrons of >3 MeV that precipitate into the atmosphere and can provide both confirmation of the inferred presence of >800 keV electron precipitation and an indication of the presence of even higher energy electrons.

The inferred presence of >800 keV electrons showed weak precipitation of >800 keV electrons (red line in Figure 3d) between 04:58 UT and 04:59 UT, concurrently with the 30-80 keV ion precipitations in Figure 3b. The count rates of precipitating electrons are less than 10% that of the trapped electrons (black line in Figure 3d). At the same time, we also found precipitation of >3 MeV electrons (Figure 3e) at rates about 100 times the background levels, and more intense than precipitation of >800 keV electrons because of the larger acceptance angle of that detector. The

latitudinal width of the electron precipitations is about 2 deg, which is slightly wider than that of ion precipitations. Since the proton aurora shown in Figure 3a is a manifestation of the flux tube where EMIC-ion interaction is occurring, precipitation of relativistic electrons into the proton aurora was the result of EMIC-electron interactions.

3. Summary and Discussion

The observations from ground and the satellite identified coincident precipitation of both tens of keV ions and MeV electrons associated with the helium-band EMIC waves. The observation of the proton aurora identified the flux tube in which EMIC-ions interactions actually occurred. It is noteworthy to note that during this event the DMSP satellite identified the plasmapause location conjugate point of Athabasca in the southern hemisphere [Sakaguchi et al., 2007]. Therefore, the coincident precipitation of ions and electrons observed by POES in the northern hemisphere occurred near the plasmapause. These aspects of the observations are consistent with theoretical suggestions of the early 1970's [Thorne and Kennel, 1971; Lyons and Thorne, 1972].

Energy-dependent scattering of relativistic electrons has been predicted theoretically: only high-energy electrons precipitate if EMIC waves resonate with electrons and cause pitch angle scattering [Summers and Thorne, 2003; Albert, 2003]. In order to confirm that the observations actually indicated EMIC-electron interactions, we calculated the pitch angle scattering coefficients for both ions and electrons using the quasi-linear approach [Albert, 2003]. A wave spectrum with a wave power peak and band width obtained from observation (Figure 2), and a typical EMIC wave amplitude of 1 nT at the geomagnetic equator, were assumed [Summers and Thorne, 2003; Albert, 2003]. The resonance conditions are largely influenced by the ambient plasma density, magnetic field intensity, and ion compositions. Two values of equatorial plasma density, 10 cm^{-3} and 100 cm^{-3}, were assumed for the calculations since these values are typical for regions near the plasmapause. The magnetic field intensity was calculated using an empirical model [Tsyganenko, 2002a, b]. Relevant thermal ion compositions of 70%H+, 20%He+, and 10%O+ were assumed for the magnetic active period [Loto'aniu et al., 2006].

Figure 4 shows the energy dependence of the pitch angle diffusion coefficients near the loss cone for protons (red) and electrons (blue). In both the 10 and 100 cm^{-3} cases, the observed EMIC waves can resonate with electrons of >3 MeV. Electrons of >800 keV can also resonate with the observed EMIC waves when the thermal plasma density is 100 cm^{-3}, but low-energy electrons of 30-100 keV are not able to do so, which is consistent with the POES observations. The scattering rate of 800 keV

156 electrons is much smaller than that of 3 MeV electrons. Also, in both cases the observed EMIC
157 waves can resonate with ions with energies from tens of keV to MeV, and the pitch angle diffusion
158 coefficient at lower proton energies is larger than that at higher energies. Again, this is consistent
159 with the POES observations for ions.
160
161 One may expect that the latitudinal width of ion precipitations should be the same as that of
162 electron precipitations if EMIC waves cause a coincident precipitation of ions and electrons, while
163 Figure 3 shows that the electron precipitation region was different from that of ions. The recent
164 RAM-simulation for the inner magnetosphere [Jordanova et al., 2008], in which the generation of
165 EMIC waves and pitch angle scattering was calculated for both ions and electrons in a
166 self-consistent manner, indicated that spatial distributions of electron and ion precipitations can
167 differ from each other even if the same EMIC waves cause the pitch angle scattering. Thus, based on
168 our simultaneous ground and satellite observations and theoretical calculations, we conclude that the
169 observed EMIC waves caused precipitation of relativistic electrons in the outer belt into the proton
170 aurora.
171
172 Theory suggests that the pitch angle scattering of high-energy electrons by EMIC waves is much
173 faster than that by whistler mode waves [Albert, 2003; Li et al., 2007], meaning that EMIC waves
174 would be important for rapid loss of relativistic electrons from the outer belt. Further statistical
175 studies are necessary to see how much EMIC waves contribute the net loss of the outer belt electrons.
176 Since EMIC waves are generated from a plasma instability involving ions with energies of tens of
177 keV, the pitch angle scattering of relativistic electrons by EMIC waves indicates that such ions drive
178 the dynamics of relativistic outer belt electrons through cyclotron resonance.

Acknowledgements.

The POES particle data are provided from the NGDC. This work was supported by Grants-in-Aid for Scientific Research (16403007, 19403010, 20740283, and 20244080) from the Ministry of Education, Culture, Sports, Science and Technology of Japan, and the GEMSIS, STEL, Nagoya University.

References.

Albert, J. M. (2003), Evaluation of quasi-linear diffusion coefficients for EMIC waves in a multi-species plasma, *J. Geophys. Res.*, **108**, 1249, doi:10.1029/2002JA009792.

Baker, D. N., R. Belian, P. R. Higbie, R. W. Klebesadel, and J. B. Blake (1987), Deep dielectric charging effects due to high energy electrons in the Earth's outer magnetosphere, *J. Electrost.*, **20**, 3-19.

Cornwall, J. M., F. V. Coroniti, and R. M. Thorne(1970), Turbulent loss of ring current protons, *J. Geophys. Res.*, **75**, 4699.

Erlandson, R. E., and A. J. Ukhorskiy (2001), Observations of electromagnetic ion cyclotron waves during geomagnetic storms: Wave occurrence and pitch angle scattering, *J. Geophys. Res.*, *106*(A3), 3883–3896, doi:10.1029/2000JA000083.

Evans, D. S., and M. S. Greer (2000), Polar orbiting environmental satellite space environment monitor: 2. Instrument description and archive data documentation, *Tech. Memo. OAR SEC-93*, NOAA, Boulder, CO..

Horne, R., and R. M. Thorne (1998), Potential waves for relativistic electron scattering and stochastic acceleration during magnetic storms, *Geophys. Res. Lett.*, **25**, 3011-3014.

Horne, R.(2007), Acceleration of killer electrons, *Nature*, 590-591.

Jordanova, V. K. et al.(2001), Modeling ring current proton precipitation by electromagnetic ion cyclotron waves during the May 14-16, 1997, storm, *J. Geophys. Res.*, **106**, 7,

Jordanova, V. K., M. Spasojevic, and M. F. Thomsen (2007), Modeling the EMIC wave-induced formation of detached subauroral proton arcs, *J. Geophys. Res.*, **112**, A08209, doi:10.1029/2006JA012215.

Jordanova, V., J. Albert, and Y. Miyoshi (2008), Relativistic electron precipitation by EMIC waves from self-consistent global simulation, *J. Geophys. Res.*, doi:10.1029/2008JA013490, in press.

Li W., Y. Y. Shprits, and R. M. Thorne (2007), Dynamic evolution of energetic outer zone electrons due to wave-particle interactions during storms, *J. Geophys. Res.*, **112**, A10220, doi:10.1029/2007JA012368.

213 Lorentzen, K. R. et al. (2000), Precipitation of relativistic electrons by interaction with
214 electromagnetic ion cyclotron waves, *J. Geophys. Res.*, **105**, 5381-5389.
215 Loto'aniu, T. M., R. M. Thorne, B. J. Fraser, and D. Summers (2006), Estimating relativistic electron
216 pitch angle scattering rates using properties of the electromagnetic ion cyclotron wave spectrum, *J.*
217 *Geophys. Res.*, **111**, A04220, doi:10.1029/2005JA011452.
218 Lyons, L. R., and R. M. Thorne (1972), Parasitic pitch angle diffusion of radiation belt particles by
219 ions cyclotron waves, *J. Geophys. Res.*, **77**, 5608-5617.
220 Lyons, L. R., and R. M. Thorne (1973), Equilibrium structure of radiation belt electrons, *J. Geophys.*
221 *Res.*, **78**, 2142-2149.
222 Meredith, N. P. et al. (2003), Statistical analysis of relativistic electron energies for cyclotron
223 resonance with EMIC waves observed on CRRES, *J. Geophys. Res.*, **108**(A6), 1250,
224 doi:10.1029/2002JA009700.
225 Millan R. M., R. P. Lin, D. M. Smith, K. R. Lorentzen, and M. P. McCarthy (2002), X-ray
226 observations of MeV electron precipitation with a balloon-borne germanium spectrometer,
227 *Geophys. Res. Lett.*, **29** (24), 2194, doi:10.1029/2002GL015922.
228 Millan, R. M., and R. M. Thorne (2007), Review of radiation belt relativistic electron losses, *J. Atm.*
229 *Solar-Terr. Phys.*, **69**, 362-377.
230 Miyoshi, Y. et al. (2003), Rebuilding process of the outer radiation belt during the November 3, 1993,
231 magnetic storm - NOAA and EXOS-D observations, *J. Geophys. Res.*, **108**, 1004,
232 doi:10.1029/2001JA007542.
233 Miyoshi, Y., and R. Kataoka (2005), Ring current ions and radiation belt electrons during
234 geomagnetic storms driven by coronal mass ejections and corotating interaction regions, *Geophys.*
235 *Res. Lett.*, **32**, L21105, doi:10.1029/2005GL024590.
236 Miyoshi Y., A. Morioka, R. Kataoka, Y. Kasahara, and T. Mukai (2007), Evolution of the outer
237 radiation belt during the November 1993 storms driven by corotating interaction regions, *J.*
238 *Geophys. Res.*, **112**, A05210, doi:10.1029/2006JA012148.
239 Reeves, G. D., K. L. McAdams, R. H. W. Friedel, and T. P. O'Brien (2003), Acceleration and loss of
240 relativistic electrons during geomagnetic storms. *Geophys. Res. Lett.*, **30**,
241 doi:10.1029/2002GL016513.
242 Sakaguchi, K. et al. (2007), Simultaneous ground and satellite observations of an isolated proton arc
243 at subauroral latitudes, *J. Geophys. Res.*, **112**, A04202, doi:10.1029/2006JA012135.
244 Sakaguchi, K. et al. (2008) Simultaneous appearance of isolated auroral arcs and Pc 1 geomagnetic
245 pulsations at subauroral latitudes, *J. Geophys. Res.*, **113**, A05201, doi:10.1029/2007JA012888.
246 Sandanger, M., F. Soraas, K. Aarsnes, K. Oksavik, and D. S. Evans (2007), Loss of relativistic
247 electrons: Evidence for pitch angle scattering by electromagnetic ion cyclotron waves excited by
248 unstable ring current protons, *J. Geophys. Res.*, **112**, A12213, doi:10.1029/2006JA012138.

249 Shiokawa, K. et al. (1999), Development of optical mesosphere thermosphere imagers (OMTI), *Earth*
250 *Planets Space*, **51**, 887.
251 Søraas, F., J. A. Lundblad, N. F. Maltseva, V. Troitskaya, and V. Selivanov (1980), A
252 comparison between simultaneous I.P.D.P. groundbased observations and observations of
253 energetic protons obtained by satellites, *Planet. Space Sci.*, 28, 387-405.
254 Summers, D., and R. M. Thorne (2003), Relativistic electron pitch angle scattering by
255 electromagnetic ion cyclotron waves during geomagnetic storms, *J. Geophys. Res.*, **108**, 1143,
256 doi:10.1029/2002JA009489.
257 Thorne, R. M., and C. F. Kennel (1971), Relativistic electron precipitation during magnetic storm
258 phase, *J. Geophys. Res.*, **76**, 446.
259 Tsyganenko, N. A.(2002a), A model of the near magnetosphere with a dawn-dusk asymmetry - 1.
260 Mathematical structure, *J. Geophys.Res.*, 107, A8, 10.1029/2001JA000219.
261 Tsyganenko, N. A. (2002b), A model of the near magnetosphere with a dawn-dusk asymmetry 2.
262 Parameterization and fitting to observations, *J. Geophys. Res.*, **107**, A8, 1176,
263 doi:10.1029/2001JA000220.
264 Yahnina, T. A., A. G. Yahnin, J. Kangas, and J. Manninen (2000), Proton precipitation related to
265 Pc1 pulsations. *Geophys. Res. Lett.*, 27 (21), 3575.
266 Yahnina, T. A., et al. (2003), Energetic particle counterparts for geomagnetic pulsations of Pc1
267 and IPDP types, *Ann. Geophys.*, 21, 2281.
268

Figure caption.

Figure 1.

(a). Photograph of the isolated proton auroral arc in the southern sky of Athabasca, Canada, taken on September 5, 2005, and the Athabasca observatory building with two all-sky camera domes on the roof. (b). An auroral image at a wavelength of Hβ line obtained by averaging images captured from 0430 to 0500 UT. The arc-like structure perpendicular to that arc is the Milky Way, as can be seen in Figure 1a. The dashed line shows the trajectory of the POES-17 footprints that are mapped onto the ionospheric altitude of 120 km. The rectangle highlights the location of the isolated proton aurora.

Figure 2.

(a). Waveform of EMIC waves during the event. (b). Power spectral density of EMIC waves. Three vertical lines in the panel indicate gyro-frequencies at the magnetic equator for hydrogen, helium, and oxygen, respectively.

Figure 3.

Emission profile of Hβ (a), and count rates of energetic ions and electrons observed by POES-17 (b-e) on September 5, 2005 with UT, MLAT, the McIlwain L-value, and magnetic local time (MLT) of the satellite footprint during the period when the satellite was crossing over Athabasca. The vertical blue line indicates the time when the satellite footprint crossed the stable isolated proton aurora. MLAT and L-value are calculated by the IGRF model.

Figure 4.

Pitch angle scattering rate of ions (red lines) and electrons (blue lines) by EMIC waves indicated by left and right axes, respectively. Solid and dotted lines correspond to the cases of thermal densities of 100 cm^{-3} and 10 cm^{-3}, respectively.

a

b

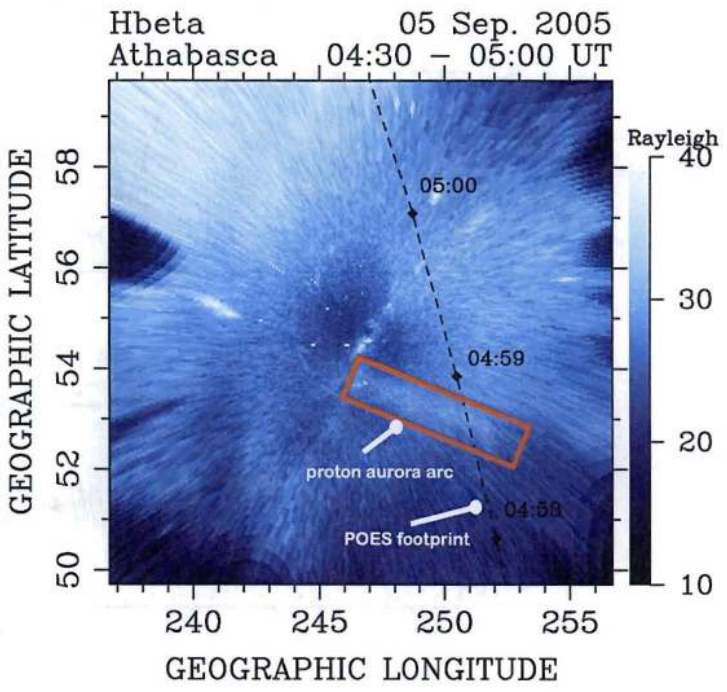
Hbeta
Athabasca
05 Sep. 2005
04:30 – 05:00 UT
Rayleigh
40
30
20
10
05:00
04:59
04:59
proton aurora arc
POES footprint
GEOGRAPHIC LATITUDE
50
52
54
56
58
240
245
250
255
GEOGRAPHIC LONGITUDE

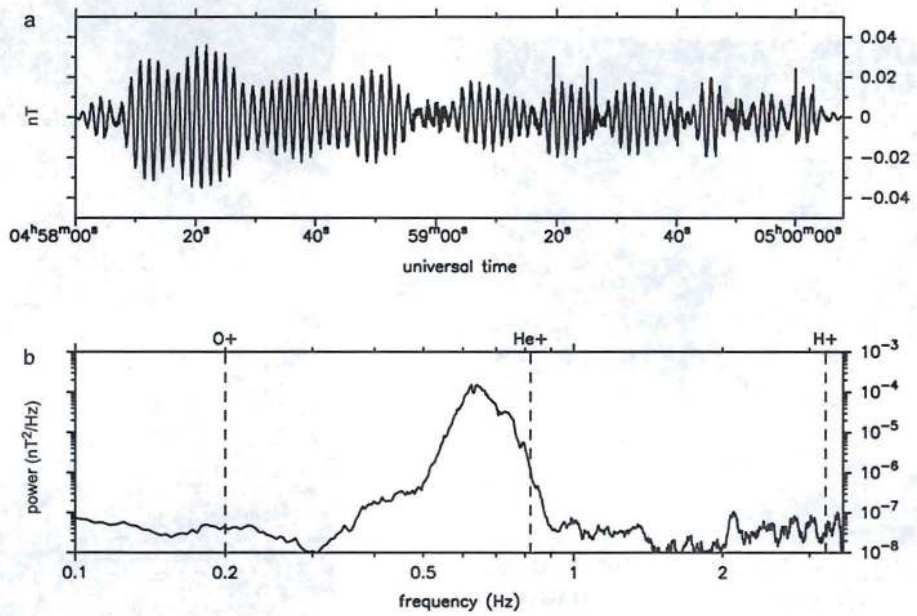
a
nT
0.04
0.02
0
−0.02
−0.04
04h58m00s
20s
40s
59m00s
20s
40s
05h00m00s
universal time
b
O+
He+
H+
power (nT²/Hz)
10⁻³
10⁻⁴
10⁻⁵
10⁻⁶
10⁻⁷
10⁻⁸
0.1
0.2
0.5
1
2
frequency (Hz)

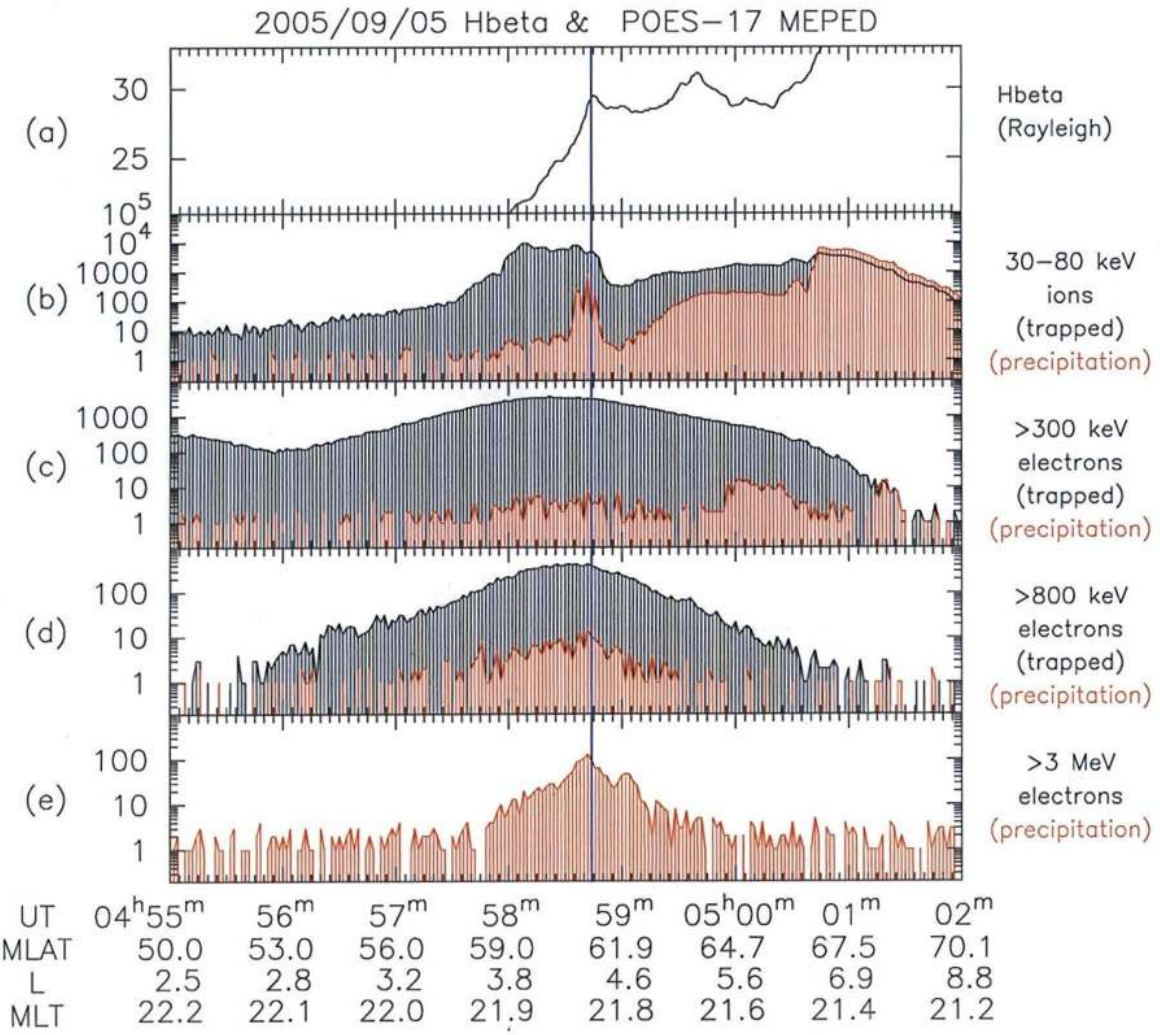
2005/09/05 Hbeta & POES−17 MEPED
(a)
30
25
Hbeta
(Rayleigh)
(b)
10^5
10^4
1000
100
10
1
30−80 keV
ions
(trapped)
(precipitation)
(c)
1000
100
10
1
>300 keV
electrons
(trapped)
(precipitation)
(d)
100
10
1
>800 keV
electrons
(trapped)
(precipitation)
(e)
100
10
1
>3 MeV
electrons
(precipitation)
UT 04h55m 56m 57m 58m 59m 05h00m 01m 02m
MLAT 50.0 53.0 56.0 59.0 61.9 64.7 67.5 70.1
L 2.5 2.8 3.2 3.8 4.6 5.6 6.9 8.8
MLT 22.2 22.1 22.0 21.9 21.8 21.6 21.4 21.2

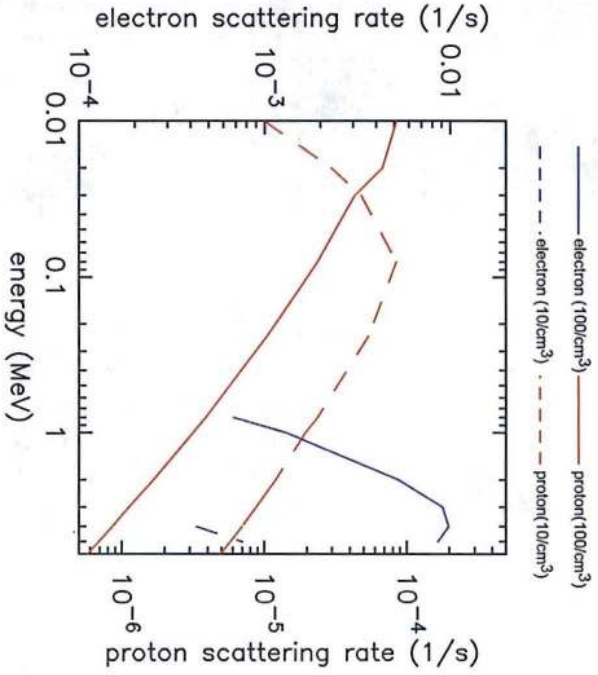
electron scattering rate (1/s)
0.01
10^{-3}
10^{-4}
0.01
0.1
1
energy (MeV)
10^{-6}
10^{-5}
10^{-4}
proton scattering rate (1/s)
electron (100/cm^3)
proton(100/cm^3)
electron (10/cm^3)
proton(10/cm^3)